1 **Supporting Information**

2 **Reaction Mechanism and Kinetics of Oxygen Reduction Reaction on the Iron-**

3 **Nickel Dual Atom Catalyst**

4

5 *Mohsen Tamtaji[1], Yuyin Li[2], Yuting Cai[2], Hongwei Liu[2], William A. Goddard III[3]*, GuanHua*

6 *Chen[1,4]**

7

8 [1]Hong Kong Quantum AI Lab Limited, Pak Shek Kok, Hong Kong SAR, China

9 [2]Department of Chemical and Biological Engineering, Guangdong-Hong Kong-Macao Joint

10 Laboratory for Intelligent Micro-Nano Optoelectronic Technology, William Mong Institute of

11 Nano Science and Technology, and Hong Kong Branch of Chinese National Engineering

12 Research Center for Tissue Restoration and Reconstruction, The Hong Kong University of

13 Science and Technology, Clear Water Bay, Kowloon, Hong Kong, 999077, P.R. China

14 [3]Materials and Process Simulation Center (MSC), MC 139-74, California Institute of

15 Technology, Pasadena CA, 91125, USA

16 [4]Department of Chemistry, The University of Hong Kong, Pokfulam Road, Hong Kong SAR,
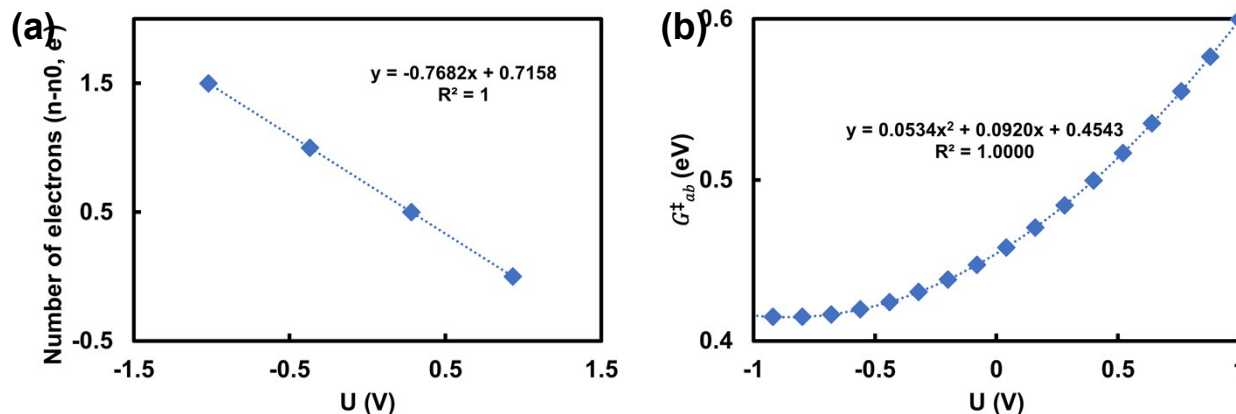
17 China

18

19

20 *Corresponding Authors, email: ghc@everest.hku.hk and wag@caltech.edu
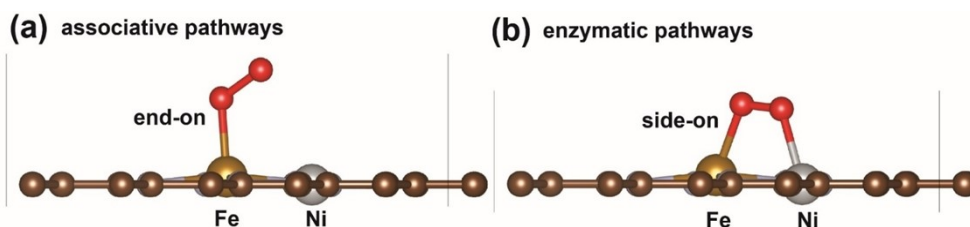
Figure S1. Adsorption of dioxygen on FeNiN6-DAC via (a) end-on and (b) side-on orientation which can lead to either associative or enzymatic pathways, respectively.
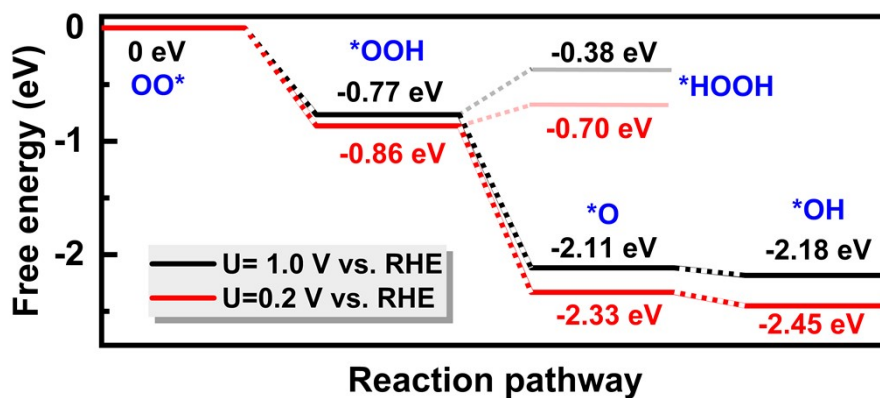
Figure S2. Free energy change of reaction intermediates at applied potentials of 1.0 V and 0.2 V vs. RHE.

Figure S3. (a) The dependence of the number of net electrons of the system as a function of applied potential. (b) The dependence of reaction barrier ($G_{ab}^{\ddagger}$) as a function of applied potential for of FeNiN6-DAC bonded to OO*. The blue dots and dash curve denote the DFT calculated energies and polynomial 2nd order fitting, respectively.
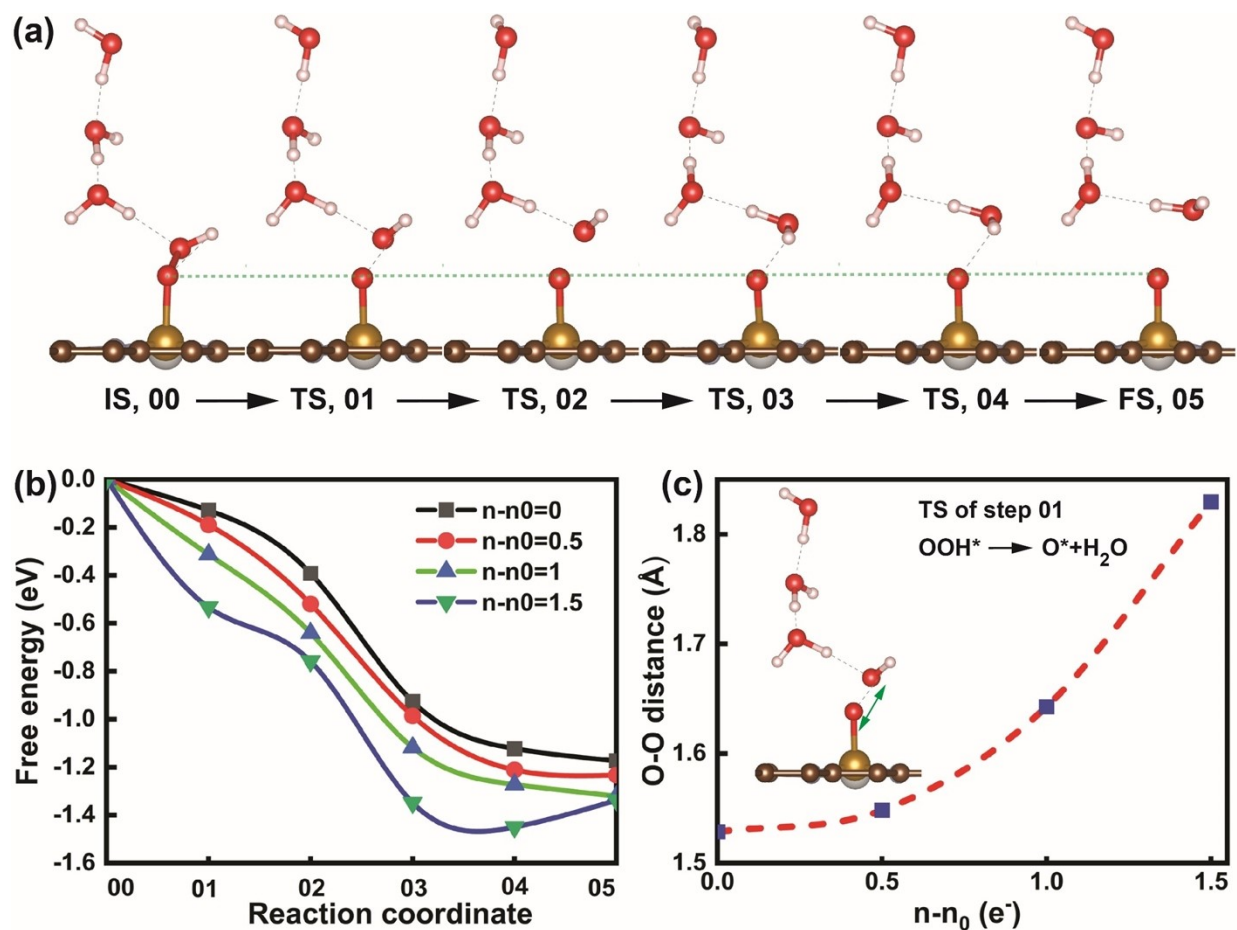
Figure S4. Investigation of transition states of $OOH^* \xrightarrow{H^+} O^* + H_2O$**.** (a) Reaction pathway of step

bc ($OOH^* \xrightarrow{H^+} O^* + H_2O$), indicating the optimized structures of initial, transition, and final states at

the applied potential of 1 V versus RHE. The transition state moves towards final state as more

negative potential applied. Four images (01-04) were inserted to search for TS, and 00 and 05

indicate the reactant and product, respectively, via minimum energy path (MEP). The dash green

lines are to show the atom displacement along the reaction pathway. (b) The free energy barrier

for the step bc ($OOH^* \xrightarrow{H^+} O^* + H_2O$) at different numbers of net electrons ($n-n_0$) in the system. It
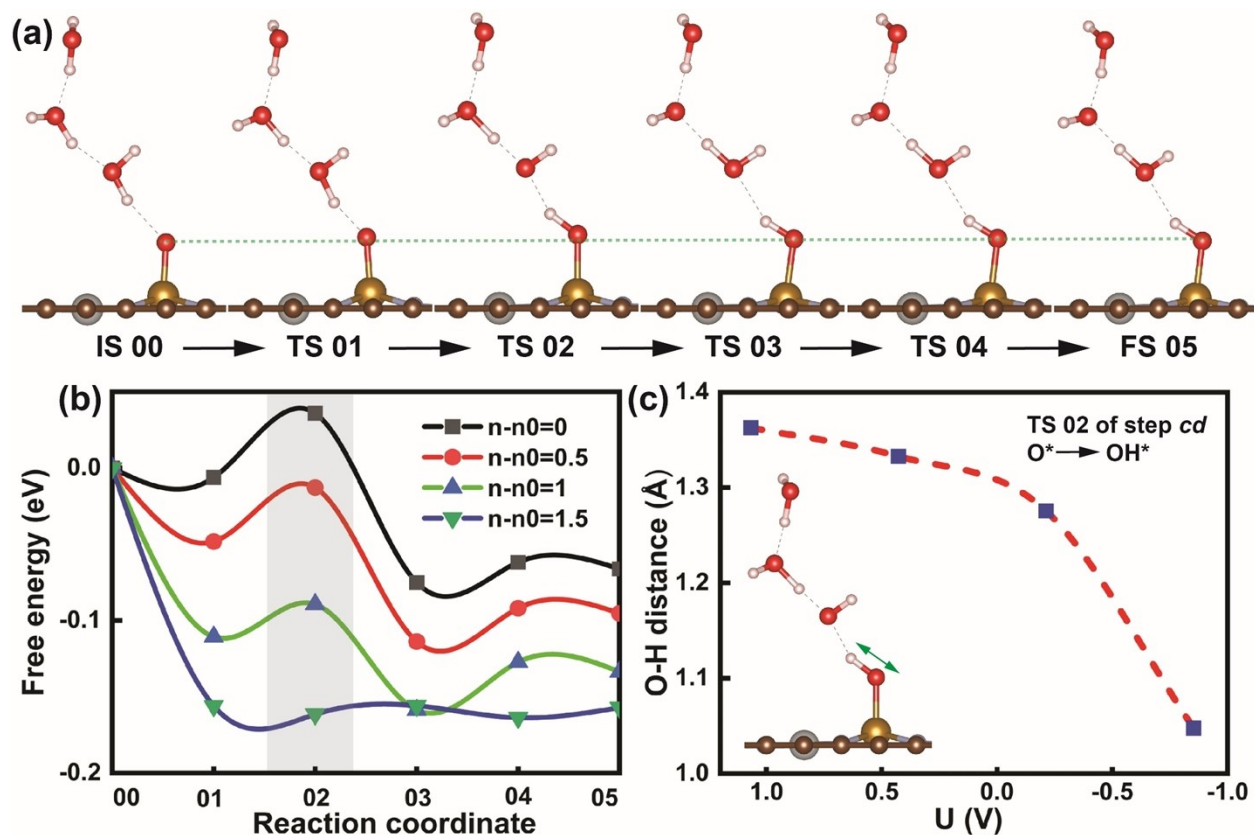
shows the maximum energy barrier of 0.00 eV and 1.2 eV at net charge of $n-n_0=0$ e^- for the forward

and backward conversion of $OOH^* \xrightarrow{H^+} O^* + H_2O$, respectively, on Fe site of FeNiN6-DAC. (c) O-O

bond distance variation of TS 01 of step bc versus the applied potential.

Figure S5. Investigation of transition states of $O^* \xrightarrow{H^+} OH^*$. (a) Reaction pathway of step *cd* ($O^* \xrightarrow{H^+} OH^*$), indicating the optimized structures of initial, transition, and final states at the applied potential of 1 V versus RHE. The transition state moves towards final state as morte negative potential applied. Four images (01-04) were inserted to search for TS, and 00 and 05 indicate the reactant and product, respectively, via minimum energy path (MEP). The dash green lines are to show the atom displacement along the reaction pathway. (b) The free energy barrier for the step 01 ($O^* \xrightarrow{H^+} OH^*$) at different numbers of net electrons (n-n_0) in the system. It shows the maximum energy barrier of 0.04 eV and 0.11 eV at net charge of n-n_0=0 e$^-$ for the forward and backward conversion of $O^* \xrightarrow{H^+} OH^*$, respectively, on Fe site of FeNiN6-DAC. (c) O-H bond distance variation of TS 02 of step *cd* versus the applied potential.
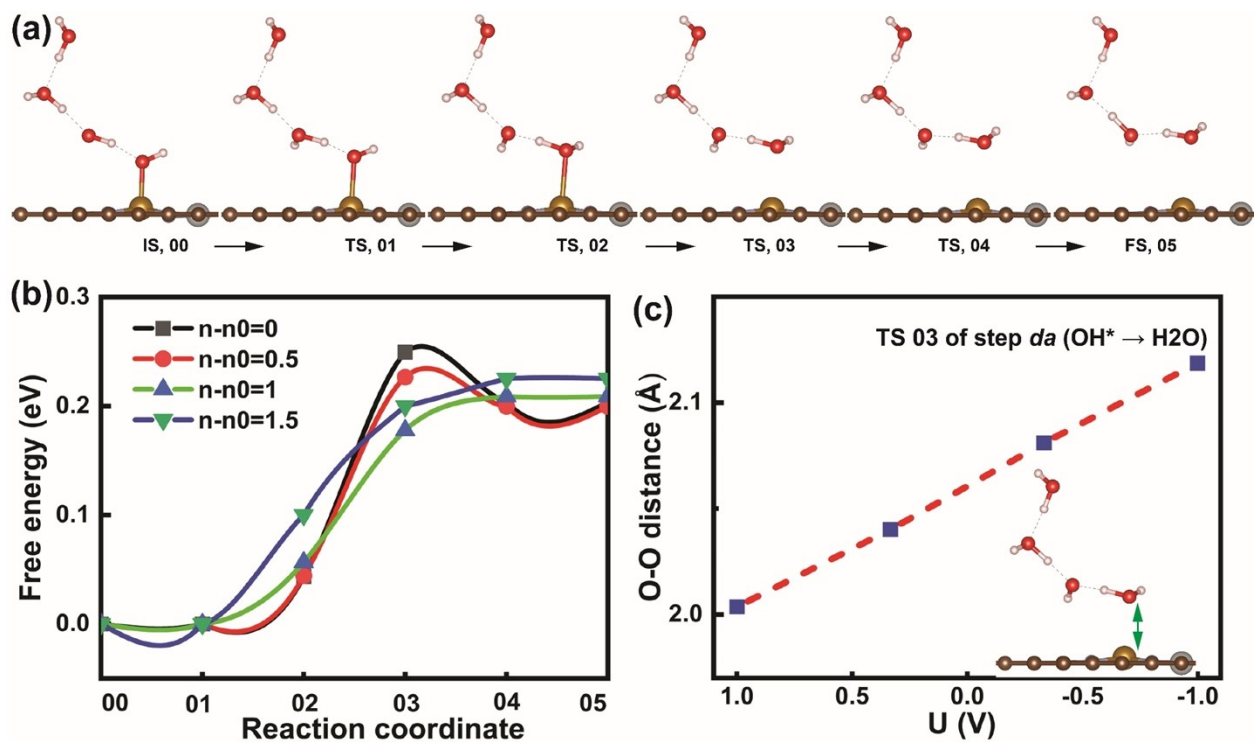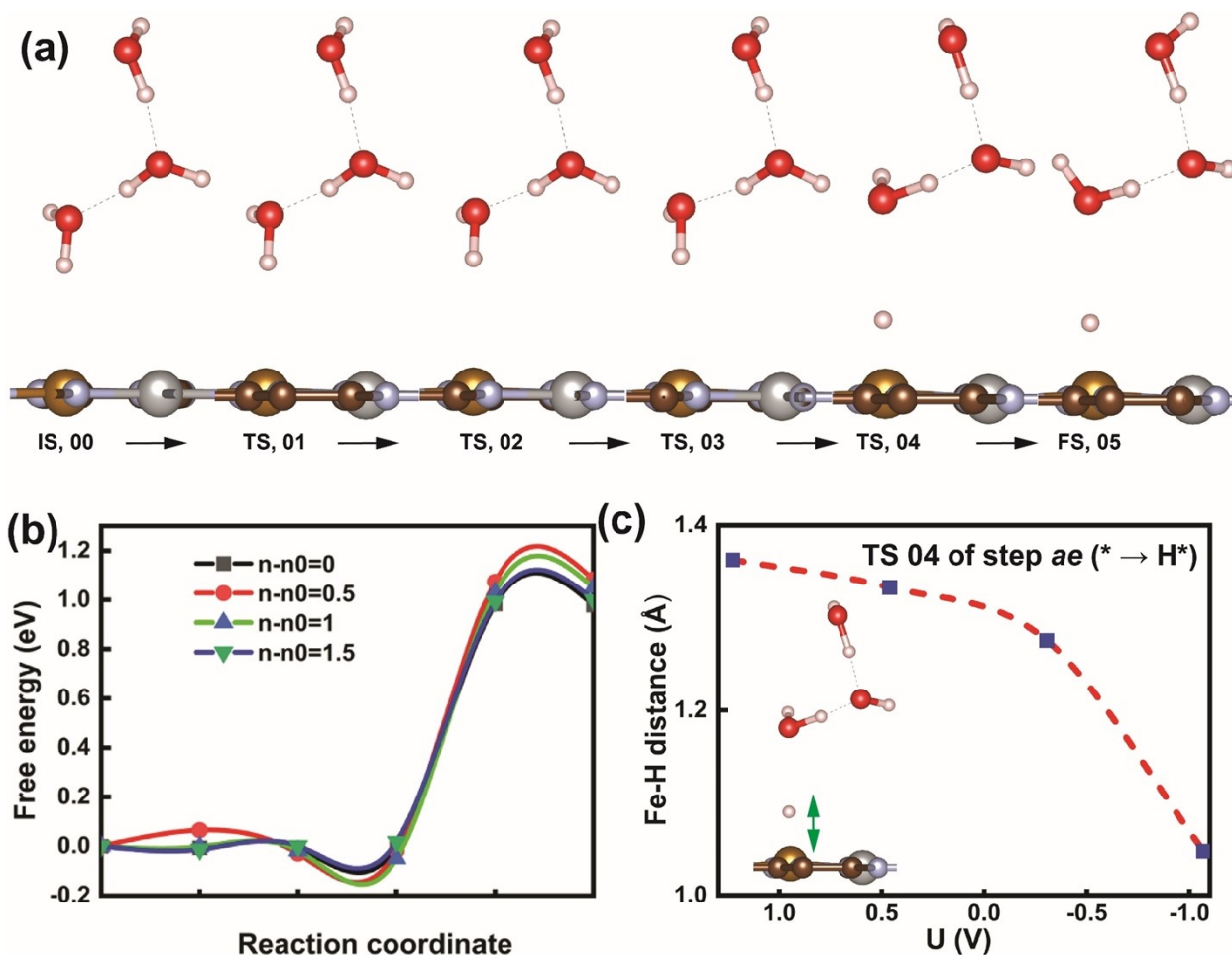
Figure S6. Investigation of transition states of $OH^* \overset{H^+}{\rightarrow} H_2O$. (a) Reaction pathway of step *da*

($OH^* \overset{H^+}{\rightarrow} H_2O$), indicating the optimized structures of initial, transition, and final states at the

applied potential of 1 V versus RHE. The transition state moves towards final state as more net

charge applied. Four images (01-04) were inserted to search for TS, and 00 and 05 indicate the

reactant and product, respectively, via minimum energy path (MEP). (b) The free energy barrier

for the step *da* (OH*→H_2O) at different numbers of net electrons ($n-n_0$) in the system. It shows

the maximum energy barrier of 0.25 eV and 0.05 eV at net charge of $n-n_0$=0 e⁻ for the forward and

backward conversion of $OH^* \overset{H^+}{\rightarrow} H_2O$, respectively, on Fe site of FeNiN6-DAC. (c) Fe-O bond

distance variation of TS 03 of step *da* versus the applied potential.

Figure S7. Investigation of transition states of $* \xrightarrow{H^+} H^*$. (a) Reaction pathway of step *ae* ($* \xrightarrow{H^+} H^*$), indicating the optimized structures of initial, transition, and final states at the applied potential of 1 V versus RHE. The transition state moves towards final state as more net charge applied. Four images (01-04) were inserted to search for TS, and 00 and 05 indicate the reactant and product, respectively, via minimum energy path (MEP). (b) The free energy barrier for the step 01 ($* \xrightarrow{H^+} H^*$) at different numbers of net electrons (n-n_0) in the system. It shows the maximum energy barrier of 1.0 eV and 0.0 eV at net charge of n-n_0=0 e^- for the conversion of $* \xrightarrow{H^+} H^*$ in forward and backward directions, respectively, on Fe site of FeNiN6-DAC. (c) Fe-O bond distance variation of TS 03 of step *da* versus the applied potential.
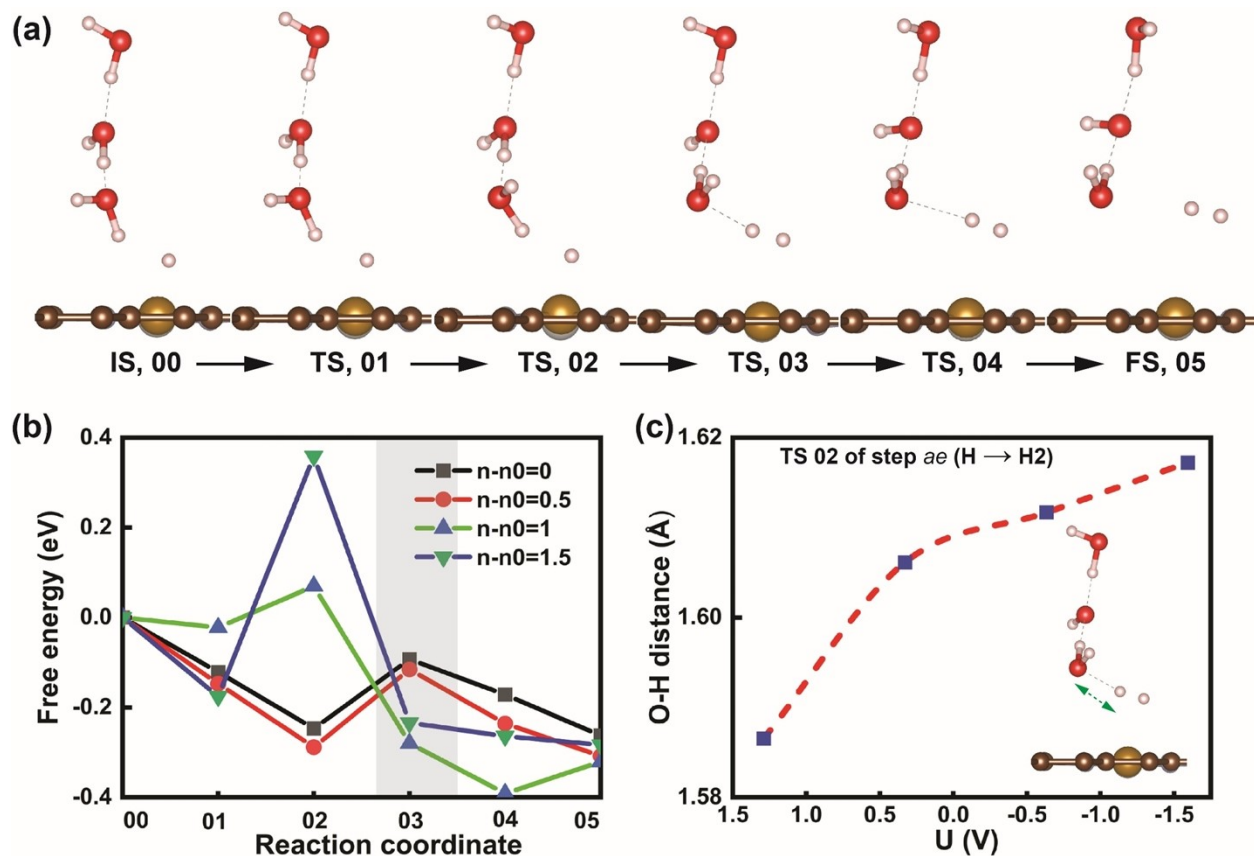
Figure S8. Investigation of transition states of $H^* \xrightarrow{H^+} H_2$. (a) Reaction pathway of step *da* ($H^* \xrightarrow{H^+} H_2$), indicating the optimized structures of initial, transition, and final states at the applied potential of 1 V versus RHE. The transition state moves towards final state as more net charge applied. Four images (01-04) were inserted to search for TS, and 00 and 05 indicate the reactant and product, respectively, via minimum energy path (MEP). (b) The free energy barrier for the step 01 ($H^* \xrightarrow{H^+} H_2$) at different numbers of net electrons ($n-n_0$) in the system. It shows the maximum energy barrier of 0.00 eV and 0.26 eV at net charge of $n-n_0=0$ e^- for the forward and backward conversion of $H^* \xrightarrow{H^+} H_2$, respectively, on Fe site of FeNiN6-DAC. (c) Fe-O bond distance variation of TS 03 of step *da* versus the applied potential.

1

2
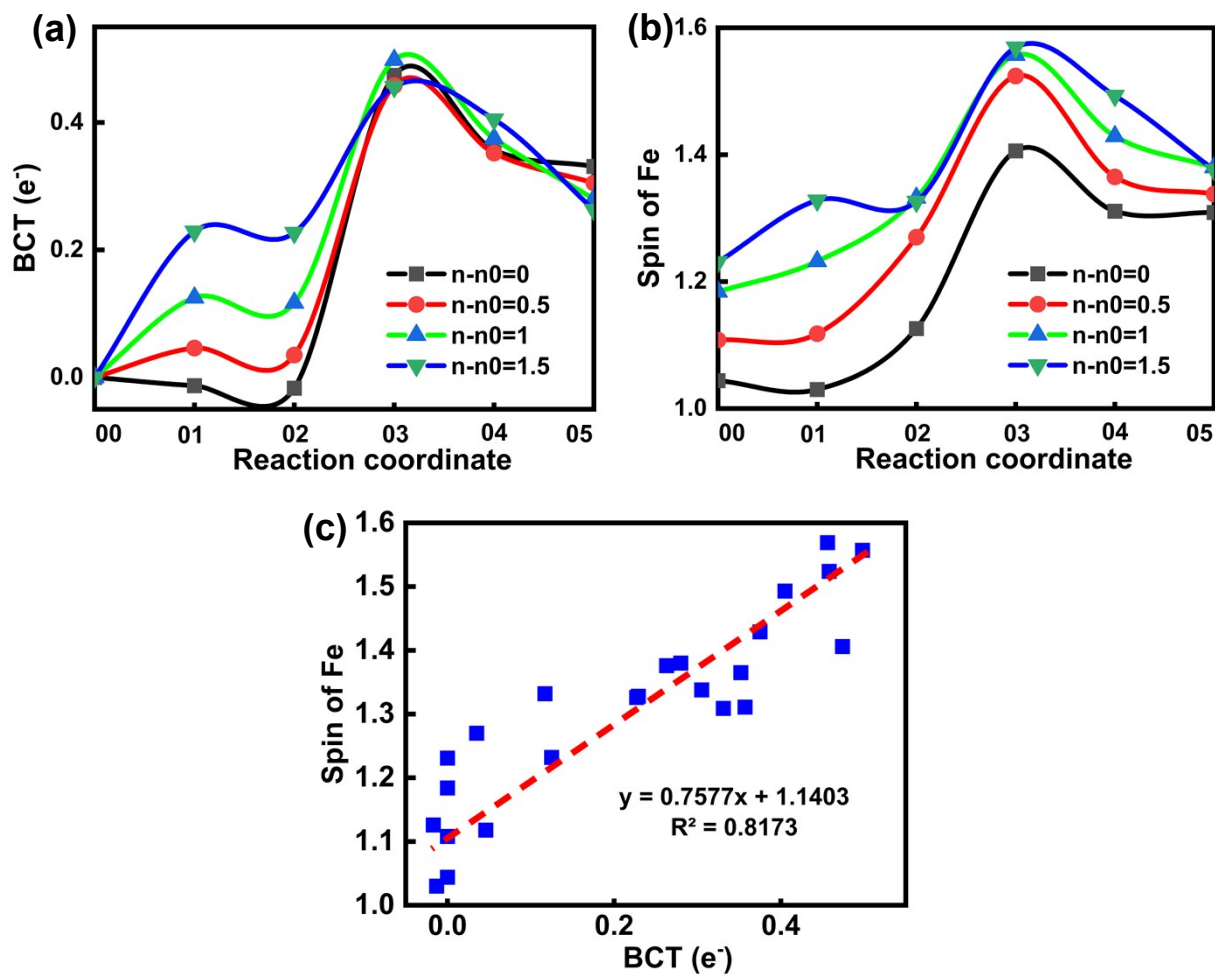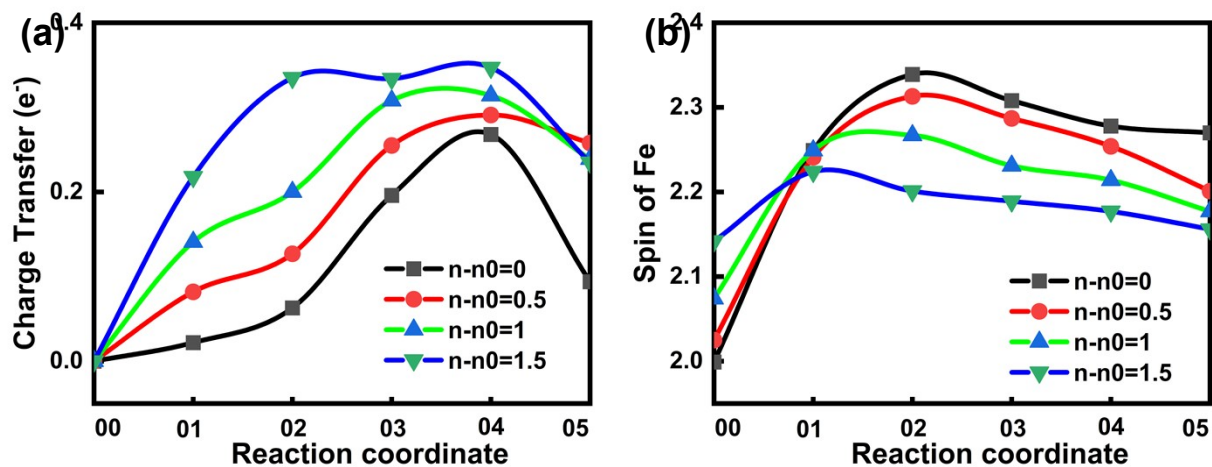
3

4

5

6 **Figure S9.** (a) Charge transfer and (b) spin of Fe versus reaction coordinate at net electrons for

7 $OO^* \xrightarrow{H^+} OOH^*$. (c) The linear relationship between the spin of Fe versus the charge transfer.
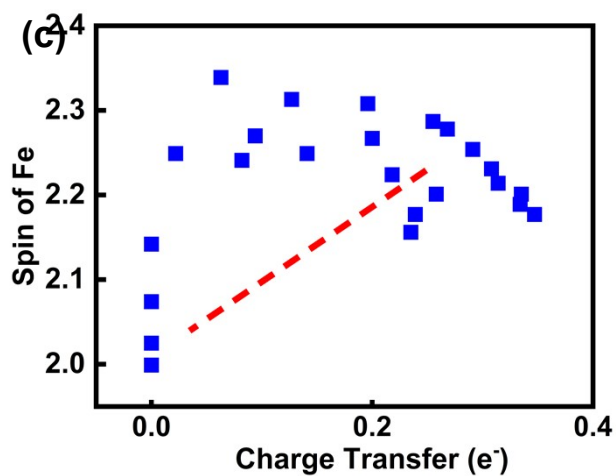
8

9

10

1

2

3 **Figure S10.** (a) Charge transfer and (b) spin of Fe versus reaction coordinate at net electrons for

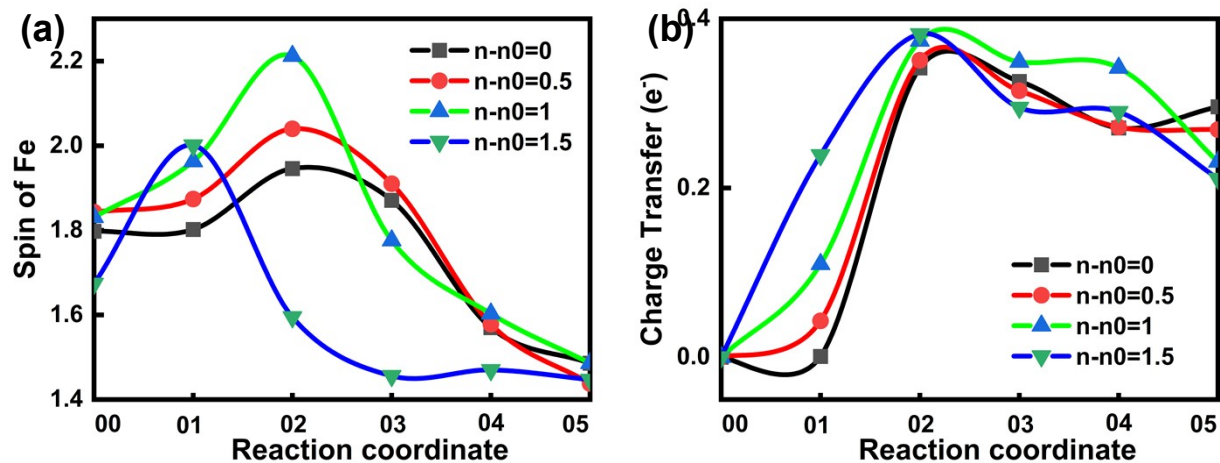4 $OOH^* \xrightarrow{H^+} O^* + H_2O$. (c) The relationship between the spin of Fe vs. the charge transfer.
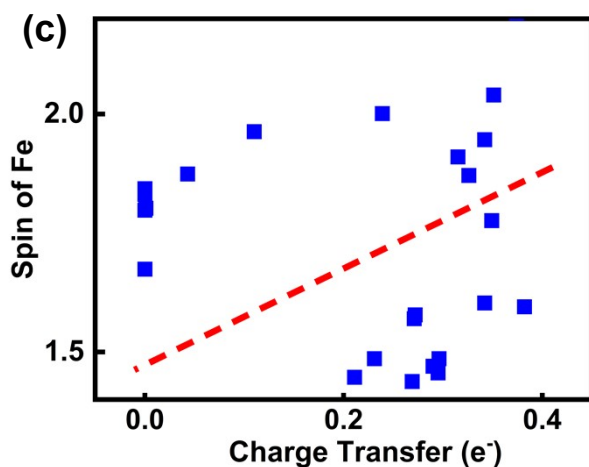
5

6

7

8

9

Figure S11. (a) Charge transfer and (b) spin of Fe versus reaction coordinate at net electrons for $O^* \xrightarrow{H^+} OH^*$. (c) The relationship between the spin of Fe vs. the charge transfer.
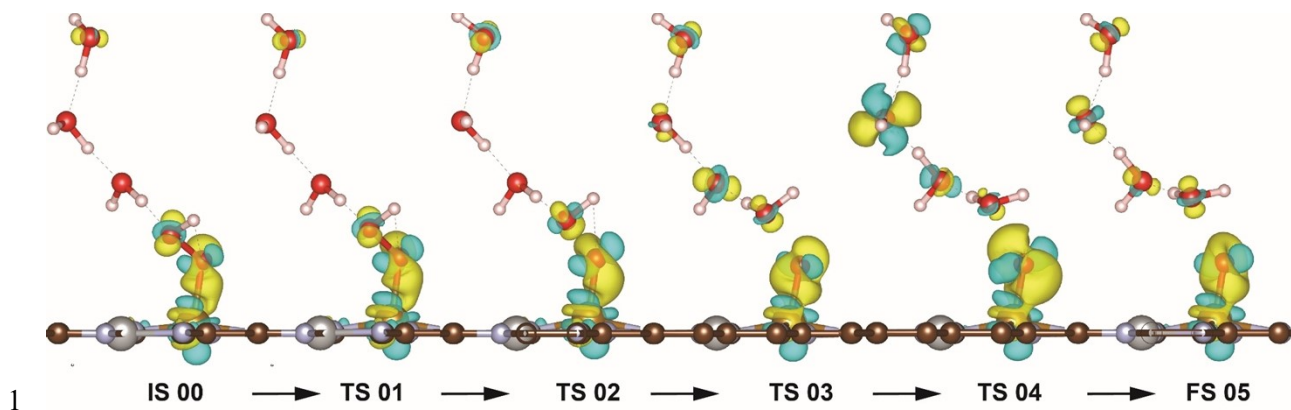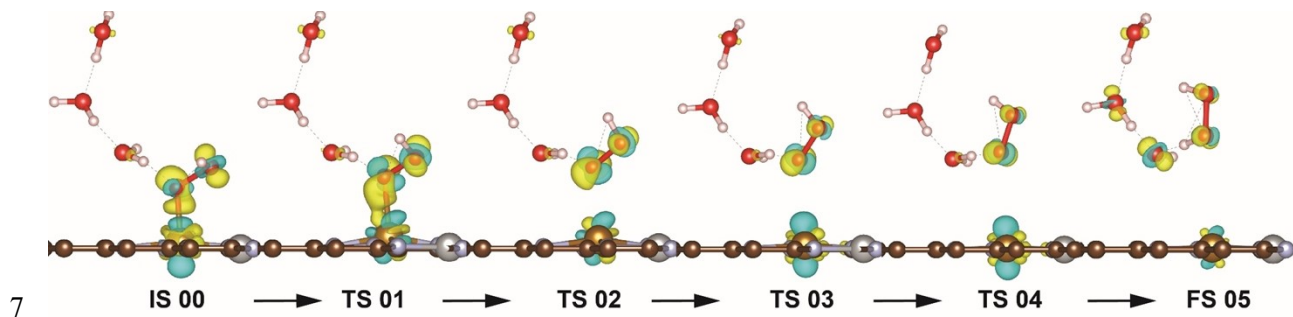
1

Figure S12. Charge transfer along the reaction pathway of step bc ($OOH^* \xrightarrow{H^+} O^* + H_2O$) at the applied potential of 1 V vs. RHE. This indicates the increase in charge transfer along the reaction pathway and proton transfer.
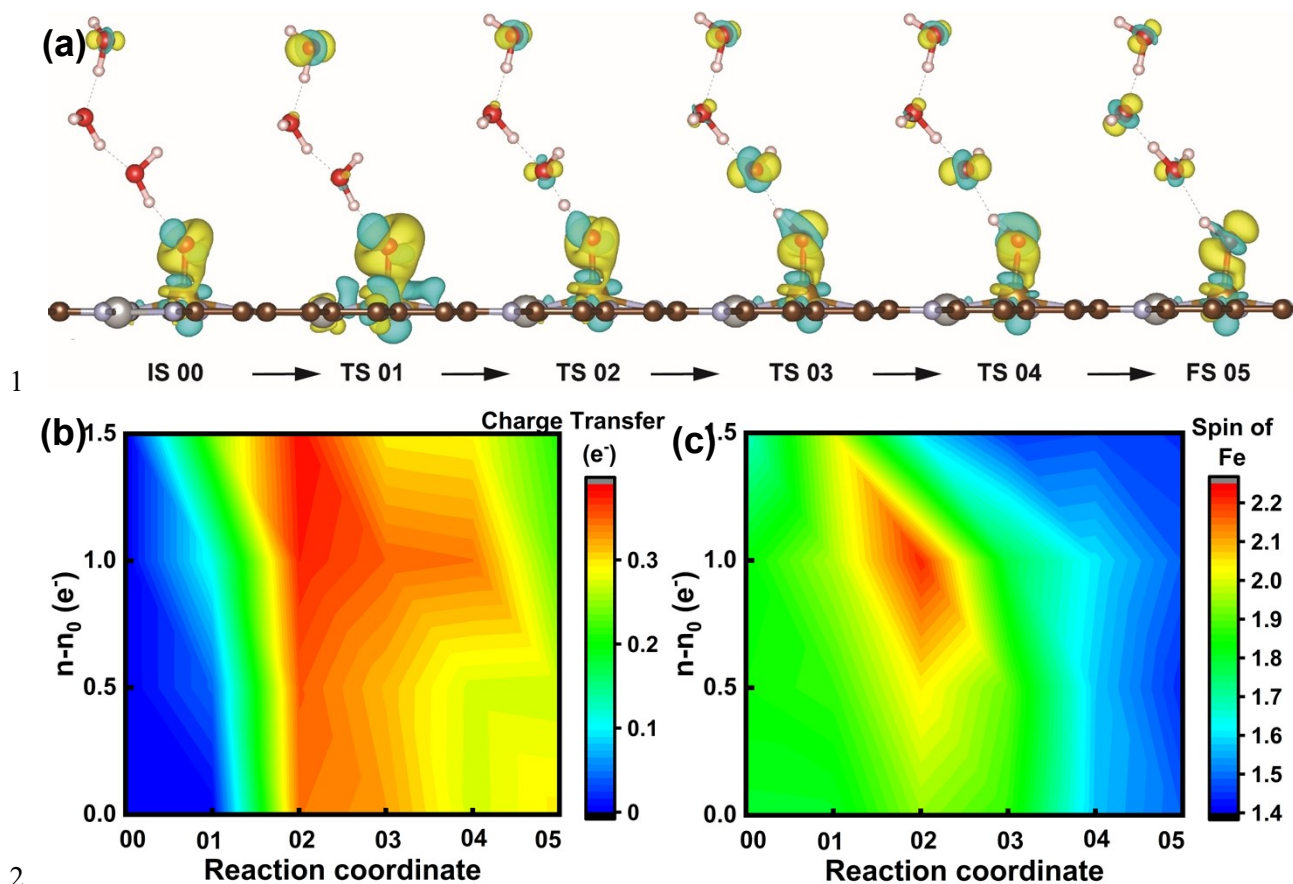

7

Figure S13. (a) Charge transfer along the reaction pathway of step ba' ($OOH^* \xrightarrow{H^+} H_2O_2$) at the applied potential of 1 V vs. RHE. This indicates the decrease in charge transfer along the reaction pathway and proton transfer.

Figure S14. (a) Charge transfer along the reaction pathway of step cd ($O^* \overset{H^+}{\rightarrow} OH^*$) at the applied potential of 1 V vs. RHE. This indicates the increase in charge transfer along the reaction pathway and proton transfer. Contour plo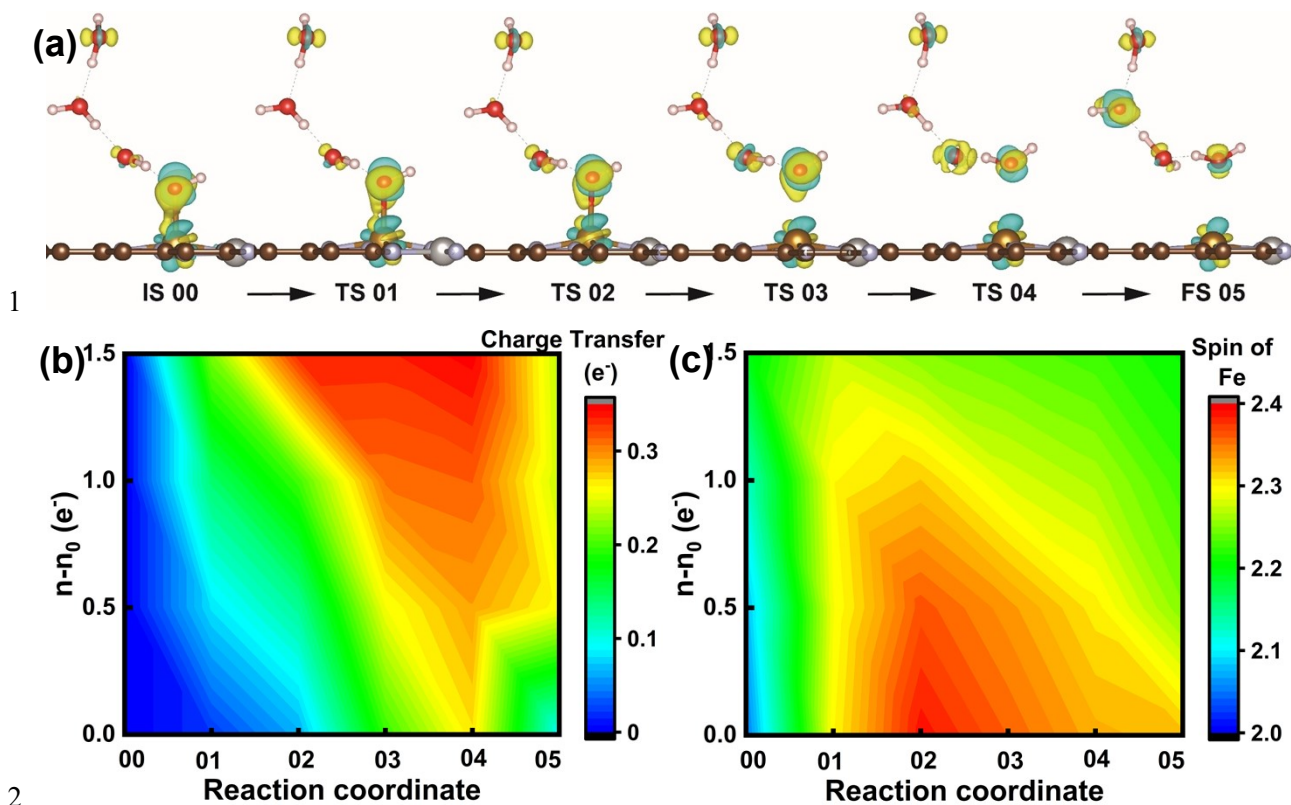t of (c) charge transfer and (d) spin of Fe versus net electrons and reaction pathway of $O^* \overset{H^+}{\rightarrow} OH^*$. This indicates that both charge transfer and spin density reach a maximum along the proton transfer.

Figure S15. (a) Charge transfer along the reaction pathway of step *da* ($OH^* \xrightarrow{H^+} H_2O$) at the applied potential of 1 V vs. RHE. This indicates the increase in charg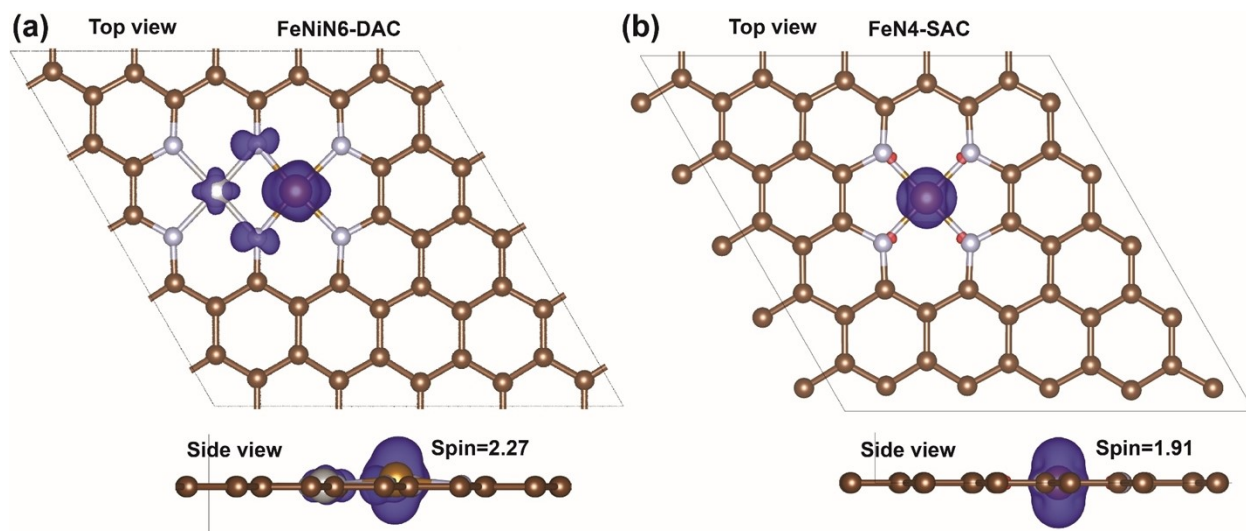e transfer along the reaction pathway and proton transfer. Contour plot of (c) charge transfer and (d) spin of Fe versus net electrons and reaction pathway of $OH^* \xrightarrow{H^+} H_2O$. This indicates that both charge transfer and spin density reach a maximum along the proton transfer.

1

2 **Figure S16.** Spin density of (a) FeNiN6-DAC and (b) FeN4-SAC, indicating the delocalization of

3 unpaired electrons of high-lying d_{z2} orbital of Fe atom into the ligands. The blue and red colors

4 represent alpha and beta spin, respectively, Isosurface value = 0.008 e/$Å^3$.
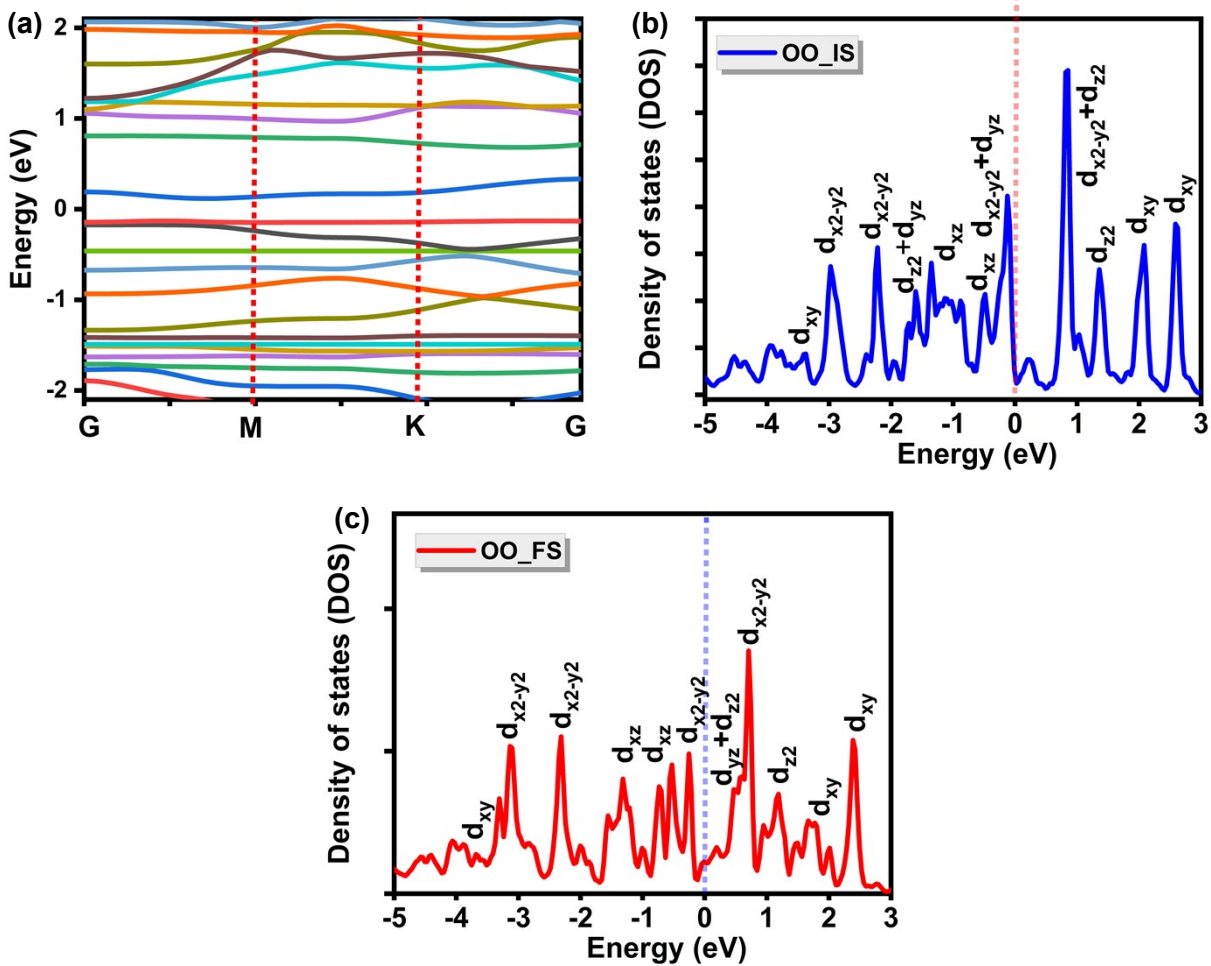
5

6

7

8

9

10

11

12

13

14

15

Figure S17. Band structure and density of states (DOS) analysis of the initial states of step

ab $OO^* \xrightarrow{H^+} OOH^*$**.** (a) The band structure and (b) density of states (DOS) of OO_IS. (c) DOS of OO_FS.
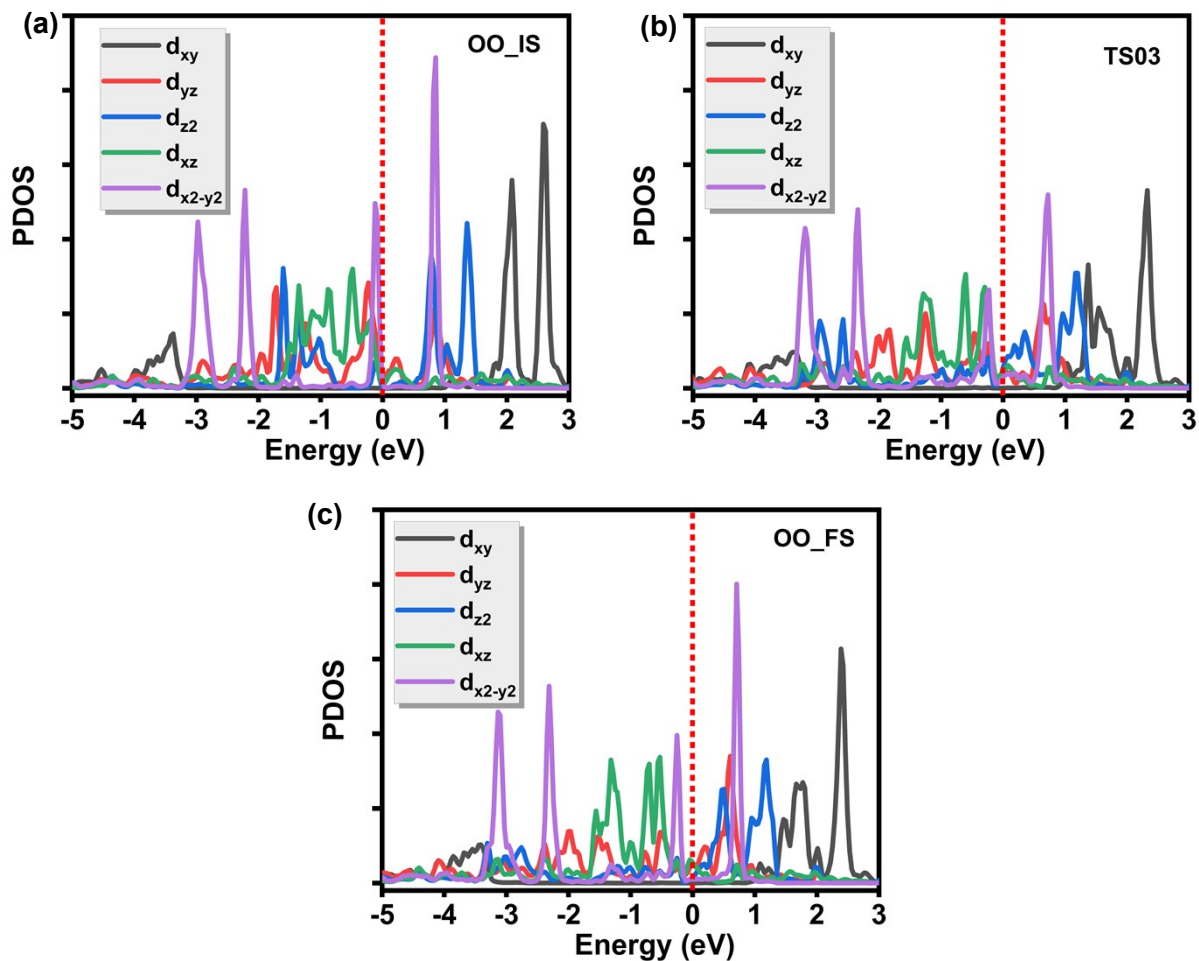
1

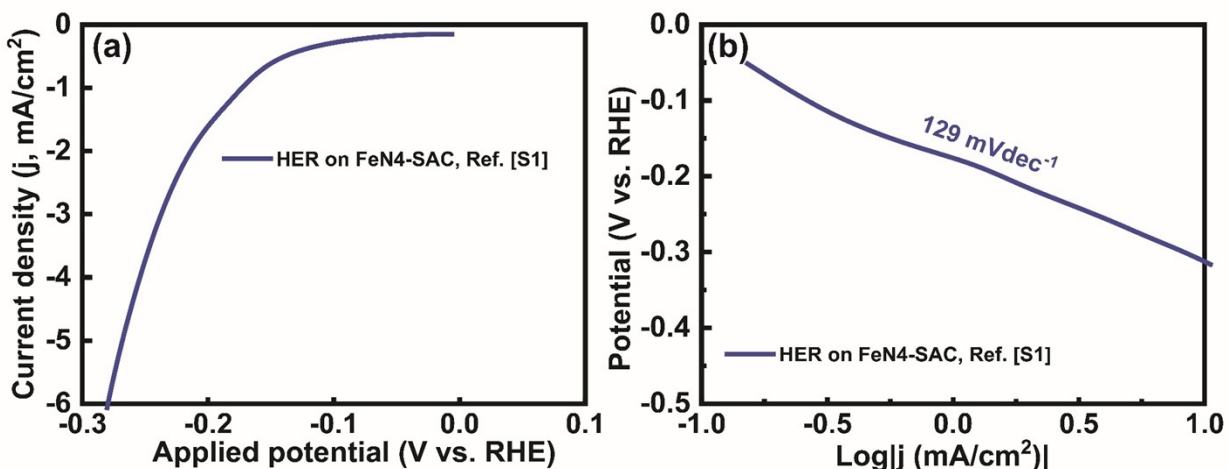
2

3

Figure S18. Partial density of states (PDOS) analysis of the final states of step *ab*

$OO^* \xrightarrow{H^+} OOH^*$. (a) PDOS of 3d hybrid orbital of Fe atom in FeNiN6-DAC for OO_IS, OO_TS03, and OO_FS.

7

Figure S19. (a) Experimental partial current densities for HER on FeN4-SAC from ref. [S1]. (b) Tafel slopes calculated from the I-V curve for HER on FeN4-SAC from ref. [S1].

Table S1. Parameters obtained from quadratic fitting to obtain the grand canonical potential.

Intermediate	$a =-\dfrac{1}{2C_{diff}}$ (eV/electron^2)	$b = \mu_{e,SHE} - eU_{PZC}$ (eV/electron)	$c = F(n = n0)$ (eV)	Vibrational contribution (eV)	U_{PZC}
O$_2$*	0.651	-5.592	-18146.838	2.073	0.932
OOH*	0.733	-5.713	-18164.822	2.372	1.053
O*	0.664	-5.630	-17712.676	1.991	0.970
OH*	0.666	-5.659	-16615.637	2.263	0.999
H*	0.879	-5.701	-17275.106	1.911	1.040

Current density calculations

Density of Fe-Ni (4.17%) = 1.326×10^{14} atoms/cm2

Current density, j(mA/cm^2)=n×F×r$_{O2}$×1000 Where, n=number of electrons transferred involved in the reaction (for O$_2$, n=4), F=Faraday's constant

r$_{O2}$ = reaction rate of O$_2$

1 **References**

2 [S1]   K. Khan, T. Liu, M. Arif, X. Yan, M.D. Hossain, F. Rehman, S. Zhou, J. Yang, C. Sun,

3   S.H. Bae, J. Kim, K. Amine, X. Pan, Z. Luo, Laser-Irradiated Holey Graphene-Supported

4   Single-Atom Catalyst towards Hydrogen Evolution and Oxygen Reduction, Adv. Energy

5   Mater. 11 (2021) 2101619. https://doi.org/10.1002/aenm.202101619.

6